



Rigorous approach for unifying wave optics and state of the art rendering techniques

TOBIAS LANGE,¹ ANNIKA VÖLL,^{1,*} MICHAEL BERENS,¹ JOCHEN STOLLENWERK,^{1,2} PETER LOOSEN,² AND CARLO HOLLY¹

¹*RWTH Aachen University TOS - Chair for Technology of Optical Systems, Steinbachstrasse 15, 52074 Aachen, Germany*

²*Fraunhofer-Institute for Laser Technology ILT, Steinbachstrasse 15, 52074 Aachen, Germany*

*annika.voell@tos.rwth-aachen.de

Abstract: With the capabilities of diffractive optics there is a rising demand for determining the light interaction of diffractive elements with arbitrary illumination and scenery. Since the structured surfaces' scale lies within the visible wavelengths and below, the light's interaction cannot be simulated with state of the art geometric optic rendering approaches. This paper presents a new model for the inclusion of wave-optical effects into Monte Carlo path rendering concepts. The derived method allows the coupling of a rigorous full-field approach with the concept of backward ray propagation through complex scenes. Therefore, the rendering of arbitrarily structured periodic optical components is now possible for complex sceneries for design, verification and testing purposes. The method's performance is demonstrated by comparing rendering results of complex sceneries including CDs with corresponding photographs.

© 2021 Optical Society of America under the terms of the [OSA Open Access Publishing Agreement](#)

1. Introduction

Since the past decade, the production methods of the semiconductor industry allow the structuring of surfaces in the nanometer scale of the visible wavelengths and below. This capability introduced a new type of optical components under the generic term of diffractive optics. These include foliations, gratings, diffractive lenses [1] and more. One of the main benefits of diffractive components is the introduction of new concepts of optical functionality, which are not attainable with conventional optical systems, while minimizing the system's size. However, these structures may have an impact on the overall part's geometry and thus aesthetic design (e.g. in headlamps) resulting in unintended color fringes or reflections.

The concept of rendering represents the key approach for the determination of an optical component's light interaction with its surrounding scenery. The basic principle of rendering is to define all elements of the scenery as geometric objects and calculate the intersections of a geometric line (ray) with the scenery's objects. Depending on the luminance representation, a scalar factor or a wavelength spectrum as well as the ray's outgoing direction are calculated at the intersection point in correlation to the geometry's material. With further determined intersections a ray path through the scenery is defined. Therefore, this process is commonly known as "path tracing". One characteristic aspect of path tracing is that, for computation efficiency, the rays are propagated inversely from the camera to the source, which is referred to as "backward raytracing" [2].

The main challenge is now to render the diffractive optical elements within their later scenery. To achieve this goal a method for defining the wave-optical effects induced by the diffractive component needs to be introduced into the rendering algorithm. However, with the already mentioned scale of the diffractive element's surface structure, complex field approaches, which fully solve Maxwell's equations, are necessary to define the light's interaction with these surfaces, instead of applying the much simpler geometric path tracing approach.

There is a wide variety of simulation approaches already available for a wave-optical solution. These include the Finite Difference Time Domain (FDTD - [3]), Rigorous Coupled Wave Analysis (RCWA - [4]), Beam Propagation Method (BPM - [5]) or the Method of Lines (MOL - [6]). However, in [7], [8] and [9] it is pointed out that a full-field calculation at runtime for every intersection point would cause a non manageable amount of computing time for rendering macro-scale sceneries.

Therefore, several authors [789789789] have developed approximate approaches for simulating wave-optical effects and combining them with path tracing, whose reduced computational effort allows these methods to be performed at the corresponding surface intersection point within the rendering algorithm. In [7], a scattering function is developed by the use of the Wigner distribution function to account for the phase propagation and therefore the wave interference. This function is only valid for a paraxial approach and is included in a state of the art rendering algorithm. It approximates rudimentary wave effects to visualize some of the color artifacts of an optical disk. In [8], wave-optical effects are induced by solving the Helmholtz equation in planar slices and using plane wave expansions to visualize randomly distributed scratches on metallic surfaces. The approach is strongly limited in geometric freedom of the diffractive structure. In [9], effects are respected by weighted samples within a spectral rendering process along with random point sampling. The key criterion for evaluating these rendering methods is to compare color shapes and gradients induced by wave-optical effects of e.g. a Compact Disk (CD) between the rendering result and the corresponding photograph of a test scenery. The published approximation methods differ significantly from the corresponding photographs in a way which makes them not usable for the simulation of more complex diffractive elements like foliations and gratings, since these elements need to be simulated by full-field approaches.

There have also been first attempts to unify the backward ray-tracing concept in rendering with rigorous diffractive simulation in which the wave-optics simulation has been performed through FDTD [10,11] or scalar diffraction theory [12]. These methods enable the rendering of diffractive elements such as metasurfaces or objects with structural color (e.g. the Morpho butterfly) and similarly treat the diffractive simulation as a surface material model within raytracing. However, there are subtle but important limitations: In the case of [10], the authors only model light incidence within one plane of incidence in their diffraction model, leading to irregularities for three-dimensional rendering. In [11], the authors simplify their material model by rescaling and bicubic interpolation of samples, to reduce the amount of data the model needs. Furthermore, because of the comparably low computing efficiency of FDTD, only a low resolution of the angular sampling is used. In [12], the diffraction simulation is only scalar and not entirely rigorous, due to a ray-based integration of light scattering within the microstructure. This results in limitations as missing knife-edge diffraction within the microstructure or the inability to simultaneously account for reflection and transmission.

On the other hand, several authors combine the RCWA with the concept of forward raytracing and focus mainly on optical systems or component design without path rendering. In these works, the RCWA is used to derive a function or a look-up table describing the spectrally resolved properties of the diffractive surface which is then used in a standard forward raytracing. Investigated properties are for example the diffraction efficiency, the transmittance / reflectance or the scattering behaviour. This idea has applications in the design of high-efficiency Light Emitting Diodes (LEDs) [13,14], in solar cells [15], in holograms [16] or in projectors [17].

Thus, no backward raytracing for path rendering has up to date been performed using RCWA [18]. As RCWA provides some significant advantages over other methods as FDTD - e.g. a direct assessment of the far field through the diffraction orders, a thorough near field investigation and a higher computation efficiency -, the full potential of rigorous wave simulations has up to date not been exploited. Furthermore, all existing methods combining wave-optical approaches with

rendering provide and present only limited possibilities for simulating the optical interaction between different components in complex sceneries.

Therefore, the goal of the presented paper is to develop an inclusion process of a full-field simulation approach based on RCWA into the backward path rendering process. The focus is set on determining and testing the diffractive optical elements' performance, setup and aesthetic design within its planned application scenery. The ray's outgoing direction as well as the resulting wavelength spectrum of an intersection should be entirely defined by the field simulation, but should additionally be performed in a Monte Carlo setup to fully use the already available methods for rendering complex scenes. To this end, the field simulation is first performed separately with discrete angles and wavelengths and then the result is coupled to the ray approach within the rendering algorithm. Herein, the specific characteristics of the RCWA simulation of evaluating diffraction orders is exploited for increased efficiency. This tool can be of use in a wide range of capabilities of optical functionality within diffractive optics as well as to omit the immense cost of prototyping in planar technology. The entire design, verification and testing steps along with a virtual image of a wide range of diffractive optical elements can be carried out with the help of the presented methods before manufacturing the first prototype.

This paper is structured as follows: Section 2 gives an overview of the field simulation component of this work followed by the derivation of the developed rendering method. Section 3 presents results and comparisons of a rendered scenery with the correlating photograph. Finally, Section 4 sums up the key elements of the proposed method as well as a few outlooks for adjoining work.

2. Methods

Concerning the rendering component of this work, color and luminance need to be represented in a wavelength dependent form, since the inclusion of wavelength dependent effects is necessary. This type of rendering is commonly known as spectral rendering [2]. The book Physically Based Rendering Technique (pbrt-v3 [2]) by Matt Pharr, Wenzel Jakob and Greg Humphreys and the corresponding freely accessible implementation pbrt-v3 present state of the art methods of the physically formulated interaction of light with arbitrary surfaces and set the base point of the presented method for rendering diffractive structures. The key benefit of pbrt concerning the goal of this work is the possibility to define a wavelength dependent spectrum for each ray.

The challenge is to identify a physically accurate correspondence between the ray model and the field representation. A self-evident possibility is the coupling of the ray as a geometric vector with an amplitude or spectrum to a homogeneous wave within the field simulation. Therefore, a simulation method based on homogeneous wave representations is necessary, where the field interaction can be determined on a periodic structure with its geometry in the scale of the incident wavelength and below.

2.1. Rigorous Coupled Wave Analysis - RCWA

With focus on computing time, Rigorous Coupled Wave Analysis (RCWA - [19]) has been chosen for the field simulation component of the presented method. Especially its direct solution character rather than an iterative one makes it suitable for performing efficient simulations of large input parameter ranges. Figure 1 shows the basic principle of RCWA for a simplified geometry.

The excitatory field of this setup consists of a homogeneous wave defined by incidence and polarization angles as well as a wavelength and an input amplitude. At first, the field in all three regions $G_{1,2,3}$ is expressed in terms of Fourier field expansions. The regions G_1 and G_3 represent infinite half spaces filled with a homogeneous material of refractive index n_1 and n_3 respectively. The region G_2 can be described as a cell of a varying refractive index along the x-axis, that repeats itself infinitely with period Λ_x along the x-axis. The geometry in the left

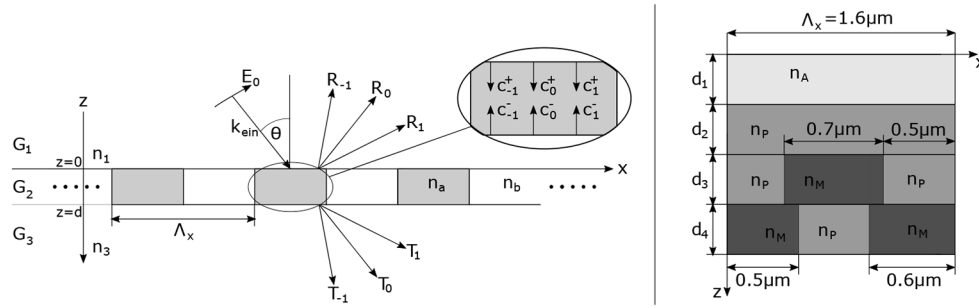


Fig. 1. The left shows the basic principle of RCWA, where a homogeneous wave of amplitude E_0 and wave vector k_{inc} is incident on an infinite 1D-periodic grating with identical cells of period Λ_x . The graph on the right represents the periodic multilayer cell-representation approximating a CD's surface as used for verification in Section 3. Here, n_A , n_P and n_M indicate the index of refraction for air, polycarbonate and aluminum respectively and $d_1 = d_3 = d_4 = 100\text{nm}$ and $d_2 = 1\mu\text{m}$.

of Fig. 1 is simplified for illustration and, as the used RCWA-package follows no restrictions concerning the geometric complexity or the used materials within the grating's periodic cell in G_2 , more complex structures, including multilayers, can be considered. The right part of Fig. 1 shows exemplarily a cell decomposition for the layer setup of the CD used in section 3. Inserting the field representations for the regions $G_{1,2,3}$ into Maxwell's equations results in an eigenvalue problem, whose solution defines the propagation terms of the corresponding field orders. By using the continuity condition of electromagnetic fields on lateral faces, the final result of the RCWA method consists of several diffraction orders, where each order defines an outgoing homogeneous wave with correlating output angles and amplitudes R_i (G_1), T_i (G_3) and c_i (G_2). This basic principle of RCWA has been developed in [19] and further extensions have been published in the following years. These include a multilayer approach [20] to account for the grating's variation along the z -axis. Furthermore, there are published concepts to handle conical wave incidence [4], 2D gratings [21] as well as several convergence optimizations. In the latter, the concept of normal vector transformation [22] in correlation to the inverse formulation [23] is a key method for the simulation of large input parameter ranges for 2D grating structures. All noted extensions as well as other self developed ones have been implemented into a 3D RCWA Python package. This package is used to perform simulations of the diffractive element's periodic cell over input parameters ranges of the incidence angles as well as the visible wavelength spectrum. The results are then saved to a local file, which is later read in by the rendering algorithm at runtime. Therefore, in the rendering step, the RCWA's results need only to be read from a local array instead of performing a full RCWA simulation at runtime. Concerning the incident azimuthal angle, the symmetry of the grating is utilized in the corresponding rendering function.

With the results of the RCWA simulation, there are now direction combinations between the incident wave and the outgoing diffraction orders available to define the ray's path at the intersection on the diffractive element's surface. Furthermore, the corresponding diffraction efficiencies represent the transition coefficient for every direction combination between incoming and outgoing ray.

2.2. BWDF derivation

The key challenge of rendering is to determine the subsequent ray direction as well as the corresponding wavelength spectrum after an intersection point between the current ray and the scenery is identified. The concept of the bidirectional distribution function (BxDF - [2]) is a widely used model for meeting these two challenges. In the following, a short introduction to the

BxDF is given before a new BxDF concept is described that includes wave-optical effects based on RCWA simulation results.

In the general case of rendering, apart from special formulations like photon mapping [2], the ray path originates at the camera point and propagates towards the light source. This backward raytracing shows key benefits in the efficiency of the rendering algorithm. At the intersection point, the camera's ray direction ω_o is flipped to point back towards the camera point. The current camera ray would now propagate further into the scene with the yet unknown direction ω_i . Both directions are formulated within the local coordinate system of the intersecting geometry. It is now physically relevant, which luminance $L_o(p, \omega_o)$ is emitted into the camera's direction ω_o at the current intersection point p . Let $L_i(p, \omega_i)$ be the yet unknown luminance at the same point p incident from direction ω_i . $L_o(p, \omega_o)$ can be formulated according to [2] by

$$L_o(p, \omega_o) = \int_{S^2} f(p, \omega_o, \omega_i) L_i(p, \omega_i) |\cos \theta_i| d\omega_i, \quad (1)$$

where S^2 describes the integration over the unity sphere's surface and $f(p, \omega_o, \omega_i)$ describes the BxDF. θ_i represents the incident polar angle between the surface normal and the incident direction ω_i .

Calculating this integral constitutes one of the main challenges of physically based rendering. Considering a simple material like a perfectly reflective mirror, only one direction ω_i in correlation to the given camera direction ω_o is evident. This follows the basic principle of the perfect reflection of mirrors. However, in the general case, all spatial directions in relation to the unit sphere contribute to the integral in Eq. (1). The Monte Carlo concept [2] is a favored method for the numerical estimation of such higher dimensional integrals. The fundamental principle for estimating the integral in Eq. (1) is to propagate only one ray from the current intersection point. The direction ω_i is chosen by a probability density function and the resulting luminance factor from direction ω_i is multiplied by a normalization factor as the integral of the chosen density function. With the use of more rays and intersections, this formulation approximates the exact solution of the integral as an estimation of Eq. (1). This principle is the key point of the luminance's estimation in this work.

One key problem of formulating the BxDF for wave-optical effects is the already mentioned "backward tracing". This tracing direction causes a problem for the field inclusion since $L_o(p, \omega_o)$ as well as the direction ω_i shall be determined by the RCWA, but the input parameters of the necessary RCWA simulation have to be derived from the yet unknown direction ω_i .

In the following, a BxDF for the integration of wave-optical effects is presented. In accordance to pbrt's implementation and nomenclature, the function is declared as BWDF (bidirectional wave density function). For simplicity, the situation of a merely reflective 1D-grating is considered, where according to Fig. 2 the intersection point of the current ray originating from the camera point is known.

Its direction ω_o in the local RCWA coordinate system of the intersected geometry's surface is represented by the black vector. From the grating's point of view, this direction must be an arbitrary outgoing diffraction order of the grating structure, for which the corresponding azimuthal ϕ_o and polar θ_o angles are calculated. At this point, it is assumed, that the direction ω_o corresponds to one out of a total amount of $N_{x,tot}$ considered diffraction orders. By neglecting higher orders with low diffraction efficiency, $N_{x,tot}$ may be smaller than the amount of diffraction orders used in the RCWA simulation itself. Nevertheless, all $N_{x,tot}$ have to be arranged symmetrically around the zeroth order of total reflection. One diffraction order $n_{x,rand}$ of $N_{x,tot}$ is chosen by using a uniformly distributed density function and the direction ω_o is assigned to this order. Furthermore, one sampled wavelength λ_{rand} is arbitrarily selected from the entire discretized spectrum of $L_o(p, \omega_o)$, since the wavelength dependence of the current path can only be expressed for one wavelength. The continuity of electromagnetic fields on boundaries defines consequentially the

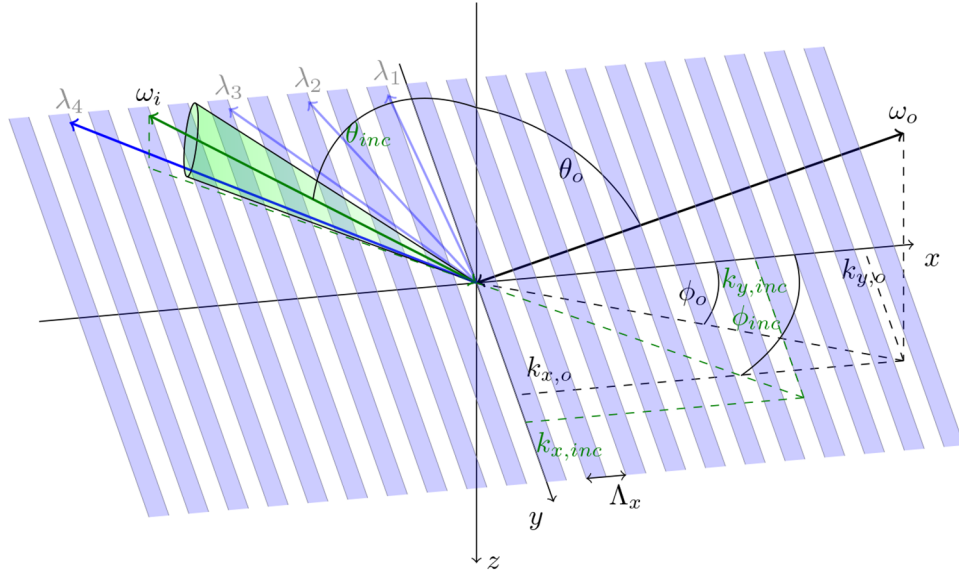


Fig. 2. The intersection of a spectral ray with a purely reflective diffraction grating.

incident ray (green - ω_i) corresponding to the outgoing ray (black - ω_o). This correspondence can be expressed by the use of the RCWA wave vector components in Eq. (2).

$$k_{x,o} = \cos \phi_o \sin \theta_o \frac{2\pi}{\lambda_{rand}} n_1, \quad (2)$$

$$k_{y,o} = \sin \phi_o \sin \theta_o \frac{2\pi}{\lambda_{rand}} n_1,$$

$$k_{x,i} = k_{x,o} + n_{x,rand} \frac{2\pi}{\Lambda_x} \quad \text{and} \quad k_{y,i} = k_{y,o}.$$

Since only 1D-gratings are considered at this point, the wave vector's y-component is invariant. Subsequently, a corresponding incoming ray of direction ω_i for the present randomized parameters of diffraction order and wavelength is defined. The Floquet condition [24] guarantees the uniqueness of this ray combination with direction (ω_i, ω_o) and the randomly chosen parameters $n_{x,rand}$ and λ_{rand} . Thus, the corresponding angles of the incoming ray can be calculated as of Eq. (3).

$$\phi_i = \tan^{-1} \left(\frac{k_{y,i}}{k_{x,i}} \right) \quad \text{and} \quad (3)$$

$$\theta_i = \begin{cases} \sin^{-1} \left(\frac{k_{y,i}}{k_0 n_1 \sin \phi_i} \right), & \text{if } |k_{y,i}| > 0. \\ \sin^{-1} \left(\frac{k_{x,i}}{k_0 n_1 \cos \phi_i} \right), & \text{if } k_{y,i} = 0 \text{ and } |k_{x,i}| > 0. \\ \pi, & \text{else.} \end{cases}$$

The necessary rotations and angle conventions in relation to the RCWA system are shown in Fig. 2. $\theta_i = \pi$ accounts for a non propagable ray with a purely real exponential base term.

With the knowledge of the incoming direction the discretized spectrum of $f(p, \omega_o, \omega_i)$ needs to be iterated since the direction ω_i is wavelength dependent. For every iterated wavelength λ_s of this spectrum the resulting diffraction order is derived to

$$N_{x,s} = n_1 \frac{\Lambda_x}{\lambda_s} (\cos \phi_i \sin \theta_i - \cos \phi_o \sin \theta_o). \quad (4)$$

In Fig. 2 there is a green cone arranged around the calculated direction ω_i for the randomly chosen order $n_{x,rand}$ and wavelength λ_{rand} , which symbolizes a case comparison for $N_{x,s}$. $N_{x,s}$ originates from a continuous set of numbers, it is therefore converted to an integer $\overline{N_{x,s,int}}$. Only if the difference between $\overline{N_{x,s,int}}$ and $N_{x,s}$ is smaller than a given threshold Δ_x and therefore lies within the green cone of Fig. 2, the resulting diffraction efficiency $DE_{LL,s}$ of the diffraction order $\overline{N_{x,s,int}}$ at this wavelength is considered. In Fig. 2, this is the case for the direction correlating to the wavelength λ_4 . The other three wavelengths (faded blue arrows) lie not within the cone and therefore don't contribute to the luminance $L_{o,s}$, which is generally derived to

$$L_{o,s}(p, \omega_o) = f_s(p, \omega_o, \omega_i) L_{i,s}(p, \omega_i) |\cos \theta_i| \quad \text{and} \quad (5)$$

$$f_s(p, \omega_o, \omega_i) = \begin{cases} DE_{LL,s} \cdot N_{x,tot} / \cos \theta_o & , \quad \text{if } |N_{x,s} - \overline{N_{x,s,int}}| < \Delta_x, \\ 0 & , \quad \text{else} \quad , \quad \text{with } \overline{N_{x,s,int}} = \text{sgn}(N_{x,s})(|N_{x,s}| + 0.5), \end{cases}$$

where the diffraction efficiency is multiplied by $N_{x,tot}$ in order to include the normalization of the uniformly distributed density function along which the diffraction order has been chosen. Since the input parameter ranges of the RCWA simulations are only discrete, there needs to be an interpolation from the continuous angles calculated in the BWDF. For this purpose, a bilinear interpolation of the diffraction efficiencies $DE_{LL,s}$ is performed with respect to the discrete upper and lower azimuthal and polar angles. This interpolation prevails as a well known method in computer graphics and a simple 2D extension of a linear interpolation [25]. Theoretically, a bicubic interpolation may be used instead, however test cases have not shown any benefits with the bicubic interpolation rather than it causing significantly more computational time than the bilinear interpolation.

The presented BWDF concept can be extended for transmitted field components as well. In this case, the negative z-component of ω_o in Fig. 2 needs to be considered in the calculation of the corresponding angles. Furthermore, a uniformly distributed choice test at every intersection is necessary to determine if the ray path is reflected or transmitted. Therefore, every coefficient DE_s is additionally multiplied by a factor of 2. Moreover, the structure needs to be simulated over the same input parameter ranges in the RCWA with a z-axis inverted setup. This extended concept is denoted as the “see through” principle since all four possible ray paths of the structure are respected.

In addition, the current BWDF implementation allows the inclusion of 2D periodic structures. In this case, another diffraction order $n_{y,rand}$ of $N_{y,tot}$ is chosen randomly within a uniform distribution at the beginning. The y-component's equation of Eq. (2) is therefore derived to $k_{y,i} = k_{y,o} + n_{y,rand}(2\pi/\Lambda_y)$ with the grating period Λ_y in the y-axis. The diffraction order with respect to the y-axis is chosen in the same way as in Eq. (4) with the corresponding Δ_y test. The resulting integer order of $\overline{N_{x,y,s,int}}$ with two indices is used in the bilinear interpolation. The factor $N_{y,tot}$ is multiplied additionally to $N_{x,tot}$ onto the returned spectrum in order to account for the uniform distribution along which $n_{y,rand}$ has been chosen.

3. Results and discussion

For testing and verification purposes of the presented unification concept, the widely used Cornell Box is appropriate. Its idea has been first presented by the Computer Science department of

the name giving Cornell University [26]. The verification box in this work has been built from sintered plates, where several color spraying layers maintain a homogeneous color and smooth surfaces of the adjoining walls, as seen in Fig. 3.



Fig. 3. The photograph of the used Cornell Box.

An array of LEDs with a wide emission angle and a nearly constant emission rate over the visible wavelength spectrum is used as the upper light source. The choice for an appropriate diffraction element is rather difficult. In a first comparison, a periodic diffractive element should be placed within the Cornell Box. The periodic cells need to be defined in the RCWA simulation. However, for commercial diffractive optical elements there is not enough information present about the periodic unit cell to be able to define the cell accurately in the RCWA simulation. For this reason, a CD has been used for testing and verification purposes, since there is a lot more information available about the explicit structuring of the CD's surface. At this point, the model assumes that the CD's data cells may be represented by a single periodic cell. Furthermore, conventional refractive glass elements are positioned in the box to induce more reflection and transmission artifacts for a precise verification.

Figure 3 shows the photograph of the Cornell Box and Fig. 4 the corresponding rendering results. The pictures have been calculated with 2045 samples per pixel at a resolution of 978 to 734 pixels. The BWDF-method uses $N_{x,tot} = 11$ diffractive orders while 31 input wavelength samples evenly distributed between 400nm and 700nm have been simulated in the RCWA. In addition, the parameters Δ_x and Δ_y used for the case comparisons in the following examples are set to 0.1. The graph on the right of Fig. 1 shows the periodic cell approximation of the CD's surface used. The refractive indices of $n_A = 1.0$ for air, $n_P = 1.5$ for polycarbonate and n_M for aluminum are used herein where n_M is wavelength dependent and complex. Furthermore, n_A and n_M surround the given cell from above and below respectively. The angle discretization step in the RCWA simulation is 2° for the polar and azimuthal angle. Concerning the azimuthal angle, the structure's symmetry is utilized and consequently, only the input azimuthal angle range from 0° to 90° is simulated in the RCWA package. The RCWA-simulation itself is set up with 61 diffractive orders and its entire simulation time is up to four hours on a desktop personal computer with Intel processor I7-3770k (16 GB RAM, 4 CPU kernels). The rendering process itself, using the precomputed RCWA-values in a 1.2GB array stored on RAM during runtime, requires 22 minutes on this PC architecture.

For the purpose of comparison, pbrt's "direct lighting"-integrator, where the direction of ω_i of a continuous BxDF material is dependent on the returned luminance weight, and pbrt's "path"-integrator without such spatial dependence are used. Furthermore, the presented BDWF-method, as an extension of pbrt, uses pbrt's texture architecture, which, in the case of the CD, is used for

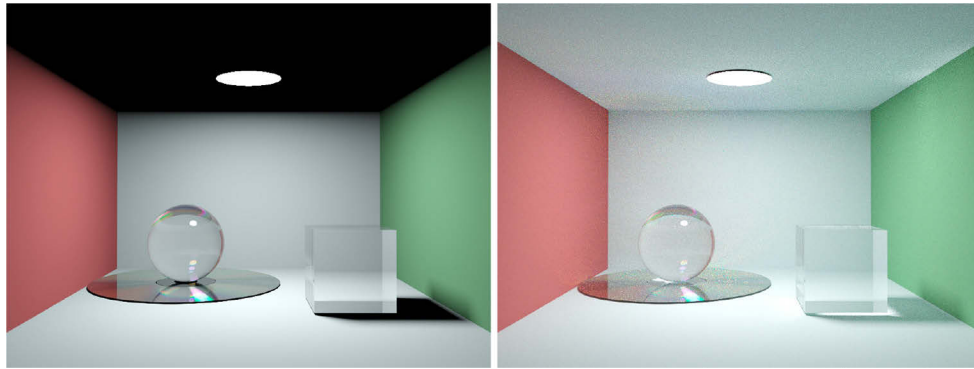


Fig. 4. The rendering result with the BWDF function for a 1D-grating shows a suitable approximation of the light's interaction onto the diffractive optical element, herein the CD. The rendered picture on the left uses pbrt's "direct lighting"-integrator, the picture on the right pbrt's "path"-integrator.

the transition into the polar coordinate system of the CD. The texture concept of pbrt allows the user to define an arbitrary rotation mapping within the input script.

It is evident that the color gradients within the use of both integrators are of identical shape and position compared to the photograph. Even the color gradient in the top left corner is visible in the rendered image created with the "path"-integrator. Therefore, both results substantiate the consistency between the rendered images and the real-world photograph.

However, the effects of the different integrators are visible as well. The "direct lighting"-integrator causes the dull ceiling to appear rather dark since it is only illuminated from ambient light and the corresponding ray paths are significantly less frequently chosen due to the already mentioned weight dependence. This effect is not existent with the use of the "path"-integrator, however this integrator induces more noise on all surfaces. It is generally presumed that the integration of the introduced BWDF as a further random process would induce a higher degree of noise in the rendered image. Nevertheless, comparing the rendering results, the degree of noise in the shadow next to the glass cube is not lower than the noise on the CD's surface. This proves that the presented BWDF method doesn't induce more noise than any other material sampling function of pbrt. Furthermore, the inclusion of the CD's RCWA sampling function doesn't require significantly more computation time than for e.g. using the sampling for a mirror or glass material in place of the CD's surface.

Figure 5 demonstrates the comparison between photograph and rendering in a second setup and view. The rendered image uses the same amount of samples and pixels as in the previous case of Fig. 4. The presented result strengthens the converging approximation of the visible wave-optical effects since the color artifacts and positions of the rendered image converge towards the photograph. However, this setup shows a few problems concerning the exact definition of the scenery in the rendering algorithm. At first, the rendered image depicts a generally higher luminance of the scene as can be seen by a comparison of the sidewall's brightness. Secondly, the photograph shows only one irradiated artifact on the CD in the lower center of the image, whereas the rendered result depicts an additional color gradient in the same region. This discrepancy is presumably caused by the camera, of which not all necessary properties are known up to this point. It is not clear, in which way the used camera handles very bright light incidence considering any scaling or clamping. Furthermore, the photograph depicts a light green artifact on the lower right corner of the CD, which is not existent in the corresponding rendered image. A possible explanation for this discrepancy is that there is a slight deviation in camera orientation or field of

view between photograph and rendered image which results in the fact that the corresponding diffraction order is not visible in the rendering.

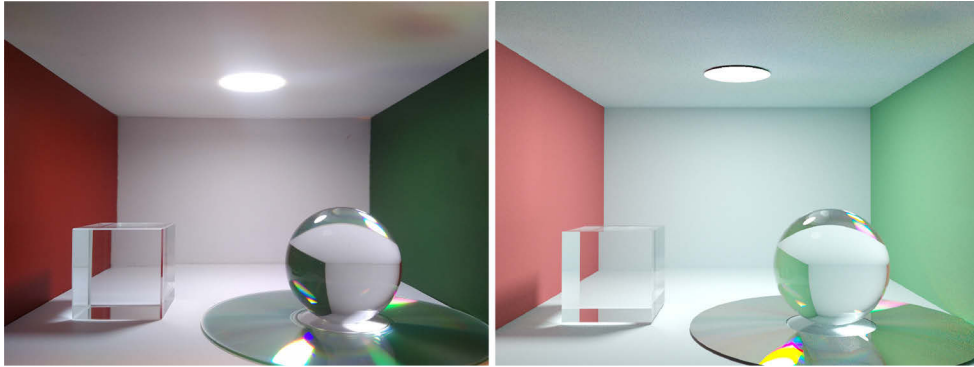


Fig. 5. The Cornell Box photograph is shown on the left, the rendering result with the BWDF function of the CD is shown on the right. The rendered result uses pbrt's "path"-integrator.

Up to this point, only a purely reflective 1D-periodic surface has been considered. As described in section 2.2 the BWDF concept can be extended to 2D periodic structures as well as to reflecting and transmitting components from both sides. An example of this "see through" principle is displayed in Fig. 6. The shown structure is a purely imaginary model. Each periodic cell with period $\Lambda_x = 1\mu\text{m}$ and $\Lambda_y = 1\mu\text{m}$ respectively and thickness $1\mu\text{m}$ consists of a centrally positioned gold plate with feed size $0.5\mu\text{m} \times 0.5\mu\text{m} \times 1\mu\text{m}$ surrounded by air. The rendered picture uses the same sampling, discretization and pixel modalities as in Fig. 4. Concerning the azimuthal angle, the structure's symmetry is utilized and consequently, only the input azimuthal angle range from 0° to 45° is simulated in the RCWA package. The gold cells are herein arranged laterally along the shown grating field. It shall be singled out that the gold gradient of the grating is purely the result of the RCWA field simulation instead of defining an object's color explicitly before runtime. This shows the capabilities of including a full-field approach solving Maxwell's equations.

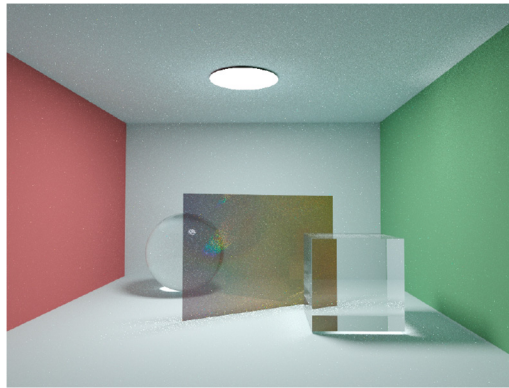


Fig. 6. The rendering result with the inclusion of the "see through" 2D-BWDF function. The "path"-integrator of pbrt is used.

4. Summary and outlook

A method for unifying spectral rendering and field simulations for complex sceneries is presented in this work. Compared to previous works, this method uses RCWA solutions to Maxwell's

equations in a backward rendering and path tracing approach, which proves, as demonstrated on the example of a CD, a high degree of conformity in the presented comparisons of photograph and rendered result. This makes the presented BWDF method suitable for optics design including the physically correct rendering of complex periodic structures with arbitrary cell design and materials. The BWDF concept induces a more accurate representation of the diffractive element and the light interaction with its surrounding scenery giving a real-life and see through image of the element. Its reduced computational effort due to the pre-computational approach in combination with the state of the art renderer pbrt suffices as a useful tool for determining the diffractive optical elements performance in its later application as well as experiencing the real life aesthetics of the diffractive optical element as a major design criterion.

Further work will contain the fine tuning of the camera parameters and the investigated diffractive element (see Section 3). Optimizations with respect to the BWDF's speedup as well as replacing the Δ_x and Δ_y test with an appropriate interpolation function are in progress. Furthermore, the inclusion of inhomogeneous luminance, which cannot be approximated by a single homogeneous wave, of only partially or non periodic structures is contemplated. With this modified field approach metalenses [27] and other diffractive structures or even entire optical systems will be traceable for design, verification and testing purposes.

Funding. Deutsche Forschungsgemeinschaft (EXC-2023 Internet of Production - 390621612).

Acknowledgements. This work is funded by the Deutsche Forschungsgemeinschaft (DFG, German Research Foundation) under Germany's Excellence Strategy – EXC-2023 Internet of Production – 390621612. Furthermore, we thank our colleague Paul Buske for proofreading this publication.

Disclosures. The authors declare no conflicts of interest.

Data availability. Data underlying the results presented in this paper are not publicly available at this time but may be obtained from the authors upon reasonable request.

References

1. L. L. Doskolovich, R. V. Skidanov, E. A. Bezus, S. V. Ganchevskaya, D. A. Bykov, and N. L. Kazanskiy, "Design of diffractive lenses operating at several wavelengths," *Opt. Express* **28**(8), 11705–11720 (2020).
2. M. Pharr, G. Humphreys, and W. Jakob, *Physically based rendering: From theory to implementation* (Morgan Kaufmann, 2017), 3rd ed.
3. A. C. Lesina, A. Vaccari, P. Berini, and L. Ramunno, "On the convergence and accuracy of the fdtd method for nanoplasmonics," *Opt. Express* **23**(8), 10481–10497 (2015).
4. M. G. Moharam, E. B. Grann, D. A. Pommet, and T. K. Gaylord, "Formulation for stable and efficient implementation of the rigorous coupled-wave analysis of binary gratings," *J. Opt. Soc. Am. A* **12**(5), 1068–1076 (1995).
5. J. van Roey, J. van der Donk, and P. E. Lagasse, "Beam-propagation method: analysis and assessment," *J. Opt. Soc. Am.* **71**(7), 803–810 (1981).
6. M. N. O. Sadiku and C. N. Obiozor, "A simple introduction to the method of lines," *Int. J. Electr. Eng. Educ.* **37**(3), 282–296 (2000).
7. T. Cuypers, T. Haber, P. Bekaert, S. Baek Oh, and R. Raskar, "Reflectance model for diffraction," *ACM Trans. Graph.* **31**(5), 1–11 (2012).
8. S. Werner, Z. Velinov, W. Jakob, and M. B. Hullin, "Scratch iridescence: Wave-optical rendering of diffractive surface structure," *ACM Trans. Graph.* **36**(6), 1–14 (2017).
9. M. Radziszewski, K. Boryczko, and W. Alda, "An improved technique for full spectral rendering," *J. WSCG* **17**, 9–16 (2009).
10. N. Okada, D. Zhu, D. Cai, J. B. Cole, M. Kambe, and S. Kinoshita, "Rendering morpho butterflies based on high accuracy nano-optical simulation," *J. Opt.* **42**(1), 25–36 (2013).
11. A. Musbach, G. W. Meyer, F. Reitich, and S. H. Oh, "Full wave modelling of light propagation and reflection," *Comput. Graph. Forum* **32**(6), 24–37 (2013).
12. V. Falster, A. Jarabo, and J. R. Frisvad, "Computing the bidirectional scattering of a microstructure using scalar diffraction theory and path tracing," in *Computer Graphics Forum*, vol. 39 (Wiley Online Library, 2020), pp. 231–242.
13. J.-Y. Na, S.-S. Yoon, Y.-B. Kim, and S.-K. Kim, "Integrated ray-wave optics modeling for macroscopic diffractive lighting devices," *Opt. Express* **27**(26), 37910–37919 (2019).
14. M. Bahl, G.-R. Zhou, E. Heller, W. Cassarly, M. Jiang, R. Scarmozzino, G. G. Gregory, and D. Herrmann, "Mixed-level optical simulations of light-emitting diodes based on a combination of rigorous electromagnetic solvers and monte carlo ray-tracing methods," *Opt. Eng.* **54**(4), 045105 (2015).
15. M. Wellenzohn and R. Hainberger, "Insights in the light trapping effect in silicon solar cells with backside diffraction gratings," *J. Photonics Energy* **3**(1), 034595 (2013).

16. H.-H. Cheng and X. Tian, "An advanced ray-tracing model for multi-color holographic optical elements," in *Holography, Diffractive Optics, and Applications IX*, vol. 11188 (International Society for Optics and Photonics, 2019), p. 1118817.
17. D. Herrmann, C. Xu, M. Bahl, and J. Jacobsen, "Modeling diffractive effects due to micro-lens arrays on liquid crystal panels in projectors," in *Photonic Instrumentation Engineering IV*, vol. 10110 (International Society for Optics and Photonics, 2017), p. 1011003.
18. J. R. Frisvad, S. A. Jensen, J. S. Madsen, A. Correia, L. Yang, S. K. S. Gregersen, Y. Meuret, and P.-E. Hansen, "Survey of models for acquiring the optical properties of translucent materials," *Comput. Graph. Forum* **39**(2), 729–755 (2020).
19. M. G. Moharam and T. K. Gaylord, "Diffraction analysis of dielectric surface-relief gratings," *J. Opt. Soc. Am. A* **72**(10), 1385–1392 (1982).
20. M. G. Moharam, D. A. Pommet, E. B. Grann, and T. K. Gaylord, "Stable implementation of the rigorous coupled-wave analysis for surface-relief gratings: enhanced transmittance matrix approach," *J. Opt. Soc. Am. A* **12**(5), 1077–1086 (1995).
21. L. Li, "Fourier modal method for crossed anisotropic gratings with arbitrary permittivity and permeability tensors," *J. Opt. A: Pure Appl. Opt.* **5**(4), 345–355 (2003).
22. T. Schuster, J. Ruoff, N. Kerwien, S. Rafler, and W. Osten, "Normal vector method for convergence improvement using the rcwa for crossed gratings," *J. Opt. Soc. Am. A* **24**(9), 2880–2890 (2007).
23. L. Li, "Use of fourier series in the analysis of discontinuous periodic structures," *J. Opt. Soc. Am. A* **13**(9), 1870–1876 (1996).
24. V. A. Yakubovich and V. M. Starzhinskii, *Linear differential equations with periodic coefficients* (Halsted Press of John Wiley & Sons, 1975).
25. I. N. Bronstein, K. A. Semendjajew, G. Musiol, and H. Mühlig, *Taschenbuch der Mathematik* (Haan-Gruiten: Verlag Europa-Lehrmittel, 2016), 7th ed.
26. Cornell University Program of Computer Graphics, "History of the cornell box," (1998).
27. M. Khorasaninejad, A. Y. Zhu, C. Roques-Carnes, W. T. Chen, J. Oh, I. Mishra, R. C. Devlin, and F. Capasso, "Polarization-insensitive metalenses at visible wavelengths," *Nano Lett.* **16**(11), 7229–7234 (2016).